



# CHORUS

This is the accepted manuscript made available via CHORUS. The article has been published as:

## Discovery of multimechanisms of screw dislocation interaction in bcc iron from open-ended saddle point searches

Xiaoyang Wang, Yifan Wang, Wei Cai, and Haixuan Xu

Phys. Rev. Materials **6**, 123602 — Published 5 December 2022

DOI: [10.1103/PhysRevMaterials.6.123602](https://doi.org/10.1103/PhysRevMaterials.6.123602)

## **Discovery of multi-mechanisms of screw dislocation interaction in bcc iron from open-ended saddle point searches**

**Xiaoyang Wang<sup>a, \*\*</sup>, Yifan Wang<sup>b</sup>, Wei Cai<sup>b</sup>, Haixuan Xu<sup>a, \*</sup>**

a. Department of Materials Science and Engineering, University of Tennessee Knoxville (UTK)

b. Department of Mechanical Engineering, Stanford University

### **Abstract**

Dislocation motion and interactions determine mechanical properties in body-centered cubic (bcc) metallic materials. However, studying mechanisms for the screw dislocation interaction is fundamentally challenging since many underlying processes involve meso-timescales and atomistic resolution, currently inaccessible by either experimental techniques or continuum theoretical methods. In this study, we develop a computational capability based on the Self-Evolving Atomistic Kinetic Monte Carlo (SEAKMC) to sample the critical events and saddle point energies related to screw dislocations and their junctions. The method is first validated by calculating the stress-dependence of Peierls barriers and formation energies of kink-pairs and cross-slip kink-pairs on a single screw dislocation in bcc iron. Then the method is applied to a binary junction of a pair of intersecting screw dislocations, the structure of which is crucial for low-temperature plastic deformation. We identify three important mechanisms: the *coplanar cross-slipping*, *jog-pinning*, and a previously unknown *unzipping* mechanism during the evolution of the binary junction. The mechanisms are then further validated using classical molecular dynamics simulations. The computational capability developed in this study provides an effective tool to evaluate screw dislocation-related thermal-activated events in complex stress conditions. The mechanisms discovered in this study provide critical insights into temperature dependence of the anomalous slip, a breakdown of the Schmidt-law, during the plastic deformation in bcc iron and can be generalized to other BCC metals.

### **Key Words**

Screw Dislocation; Binary Junction; Saddle Point Search; Kinetic Monte Carlo; Molecular Dynamics; Anomalous slip

*\*\* Visiting Scholar*

*\*Corresponding Author. Email: xhx@utk.edu*

## **1. Introduction**

During plastic deformation of body-centered cubic (bcc) metallic materials below their recrystallization temperatures, the multiplication of gliding dislocations and their interaction with other dislocations [1] contribute significantly to strain hardening. When two dislocations with  $\frac{1}{2}\langle 111 \rangle$  Burgers vectors intersect each other, a binary junction with a  $\langle 100 \rangle$  Burgers vector can form spontaneously [1]. These binary junctions are expected to act as strong barriers to dislocation motion and thus provide resistance to plastic deformation. The formation of junctions could further result in forest hardening, which plays a significant role in the overall strain hardening processes [2,3].

Based on the continuum elasticity theory, numerous discrete dislocation dynamics (DDD) studies have been conducted to understand the effects of binary junctions on strain hardening during plastic deformation [4-6]. However, the general rules of DDD simulations of binary junctions require prior knowledge of detailed dislocation reaction mechanisms, which are generally not fully known. A commonly used method to obtain the reaction mechanisms with atomistic resolution is classical molecular dynamics (MD) simulations. Though the number of atomistic studies concerning binary junctions is small, they revealed distinct interaction mechanisms under different situations. For instance, Cai [7] et al. discovered a nodal effect of dislocation motion in Molybdenum using MD, wherein screw dislocations move at lower stress in the mutual slip-plane of screw dislocations in the binary junction rather than that of the isolated screw dislocation. Raabe [1] et al. studied the hardening effect on a sliding edge dislocation by the interaction with intersecting screw dislocations in bcc iron. They quantified the obstacle strength of an intersecting dislocation and made comparisons among the obstacle strengths of other dislocation-type or inclusion-type obstacles. In addition, Xia [8] et al. studied the hardening due to the intersecting of a screw dislocation with another screw dislocation

gliding on the (112) slip-plane in niobium. They studied the junction evolution mechanisms and quantified the effect of strain rate (higher than  $\sim 10^7/s$ ) on the interaction mechanisms. Although the mechanisms and quantifications in these studies can serve as mechanistic input to the DDD simulations on binary junctions, a wide range of junction behavior is still missing. For example, what are the interaction mechanisms? What are the critical events controlling these mechanisms? And how does the presence of a binary junction affect other well-known dislocation behaviors? Therefore, further simulations are required to answer the above questions.

However, obtaining a comprehensive picture of the potential mechanisms on the binary junction is far beyond the capability of conventional atomistic simulations, e.g. classical MD. Classical MD is severely limited by its accessible timescales since MD spends most of its computational cost on vibrational events [9]. Two challenges arise from this limitation: 1) exceedingly high strain rates (over  $\sim 10^6/s$ ) compared to experiments, and 2) rare sampling of thermally activated processes with a significant energy barrier. For example, screw dislocation motion, which controls plastic deformation of bcc metals at low temperatures [10-12], occurs mainly via a thermally activated mechanism involving kink-pair nucleation and propagation [13] with an activation energy barrier ranging from 0.6 eV (for Niobium [14]) to 2.05 eV (for Tungsten [15]), as measured by experiment. Such events can be costly to sample using conventional MD. As a result, the stress-strain response calculated by classical MD may not be directly compared to experimental results.

To overcome the limitations of MD and capture the essential kinetics of thermally activated processes of screw dislocations, several approaches have been developed, such as accelerated dynamics [16], on-the-fly kinetic Monte Carlo (KMC) [17-19], and Autonomous Basin Climb (ABC) [20,21]. For example, Stukovski et al. [17] used an atomistically informed KMC algorithm to simulate the motion of a screw dislocation in tungsten via the kink-pair mechanism, with the kink-pair formation energy calculated by the nudged elastic band (NEB) method [22,23]. In this case, NEB works quite efficiently for the motion of a single dislocation because the final state of the process is known *a priori*. However, for complex systems such as dislocation binary junctions, thermally activated events could take the system to previously unknown final states, making the NEB method not applicable. KMC simulation in systems that

may potentially evolve into unknown states requires on-the-fly calculation of activation energies and structures of these states, which calls for open-ended saddle point search (SPS) algorithms to find the relevant transition states given an initial configuration. An example of open-ended SPS algorithms is the ABC method, which was used successfully by Fan[21,24] et al. to study the interaction between an edge dislocation and a nano-void at a strain rate of  $10^2 \text{ s}^{-1}$ . Fan [25] et al. have also used the ABC method to simulate screw dislocation motion via the Peierls mechanism (which assumes a dislocation moves forward as a straight line) at a low strain rate. However, the existing applications of the ABC method have not included the kink-pair mechanism or dislocation junctions. One of the underlying challenges is to sample saddle points considering a larger number of degrees of freedom. For instance, the number of atoms in the simulation systems is on the order of  $\sim 10^5$  atoms. As the number of atoms increases, the chances of successfully locating a saddle point becomes too low to be acceptable, making the simulation inefficient and unsuitable for sampling the screw dislocation junction.

To efficiently sample the rare events critical to the binary junction evolution, we develop a new computational capability based on the Self-evolving atomistic kinetic Monte Carlo (SEAKMC) [18,26] to conduct open-ended SPS and energy landscape sampling of screw dislocations and their junctions. A well-studied single-element system, bcc Fe, is used as the testing ground for the developed capability. First, we present the benchmark results of single dislocation motion by both the Peierls and kink-pair mechanisms against the NEB method. We then explore the energy landscape of a binary junction consisting of two intersecting screw dislocations, with an external strain applied to provide a maximum resolved shear stress on one (the gliding) dislocation such that it moves on the  $[111]/(1\bar{1}0)$  slip system. This dislocation interaction structure is typical in binary junction-induced strain hardening. Using SEAKMC, we obtained critical saddle point configurations related to different mechanisms exhibited by these dislocations. These mechanisms are further confirmed using classical MD at different temperature/stress conditions. We believe that these findings contribute to a mechanistic understanding of how screw dislocations interact with each other during low-temperature plastic deformation and can be related to experimental phenomena such as the temperature dependencies of anomalous slip. This work also demonstrates the feasibility of extending

atomistic simulations to meso-timescale on complex systems controlled by dislocation-mediated, thermally activated processes.

## 2. Methodology

### 2.1 SEAKMC saddle point search

SEAKMC [18,26] is an integrated on-the-fly KMC algorithm that combines saddle point search (SPS), kinetic Monte-Carlo time evolution, and relaxation. SEAKMC has many successful applications in the evolution of point-defects clusters [26-28]. In the computational capability described in this paper, we use only the *saddle\_point\_search* module of SEAKMC, modified to suit the purpose of SPS for screw dislocation and their junctions. During the SPS for Peierls barriers, a thin-slab sample is used. The box size is set up with 12.36 Å, 200 Å, and 200 Å in X, Y, and Z directions, respectively. The  $\langle 111 \rangle$  direction of the sample is set along the X direction of the box, while the  $\langle 11\bar{2} \rangle$  and  $\langle 1\bar{1}0 \rangle$  directions of the sample are set along the Y and Z directions, respectively. During the SPS for kink-pair formation energy under stress, the box size is set up as 247.27 Å × 200 Å × 200 Å, while the directions remain the same as in the Peierls barrier case. In both cases, a periodic boundary condition is set for the X direction, and free boundary conditions are set for the Y and Z directions.

To efficiently perform SPS involving a large number of atoms, we conduct Dimer [29] searches together with a localization technique, the Active Volume (AV) [27]. To determine the Peierls barrier for short dislocation samples, a cylinder shape is chosen for the AV with an axis aligned along the dislocation Burgers vector, while for long dislocations and dislocation junctions, a capsule shape covering the area of interest is chosen as an AV, with the long axis aligned along the line direction of the gliding dislocation. The convergence of saddle point energy over varying active volume sizes is tested for each saddle point found. The convergence criterion for the convergence is set to 0.001 eV. The MCM-2011 potential [13] is employed in all SPSs in

the manuscript. This potential well predicts the correct structure of the screw dislocation core and saddle point energy, meanwhile presenting the single-humped shape of the energy landscape for screw dislocations migration.

During the SPS, the dimer separation is set to be 0.001 Å. The maximum and minimum rotation forces in the dimer search are 0.1 eV/Å and 0.001 eV/Å, respectively. The maximum step size during the dimer translation using the conjugate-gradient method is 0.003 Å. The energy convergence criterion of the dimer searches is  $10^{-5}$  eV.

## 2.2 Construction of a screw dislocation junction

A screw dislocation binary junction is created by applying external strain to drive one straight screw dislocation athermally gliding toward another straight intersecting screw dislocation with a different Burgers vector. When the two dislocations get close, the junction could form spontaneously and ties the two dislocations with the dislocation reaction:  $\frac{1}{2}[111] + \frac{1}{2}[\bar{1}\bar{1}1] = [001]$ . [27] The resultant binary junction is shown in Fig. 1(a).

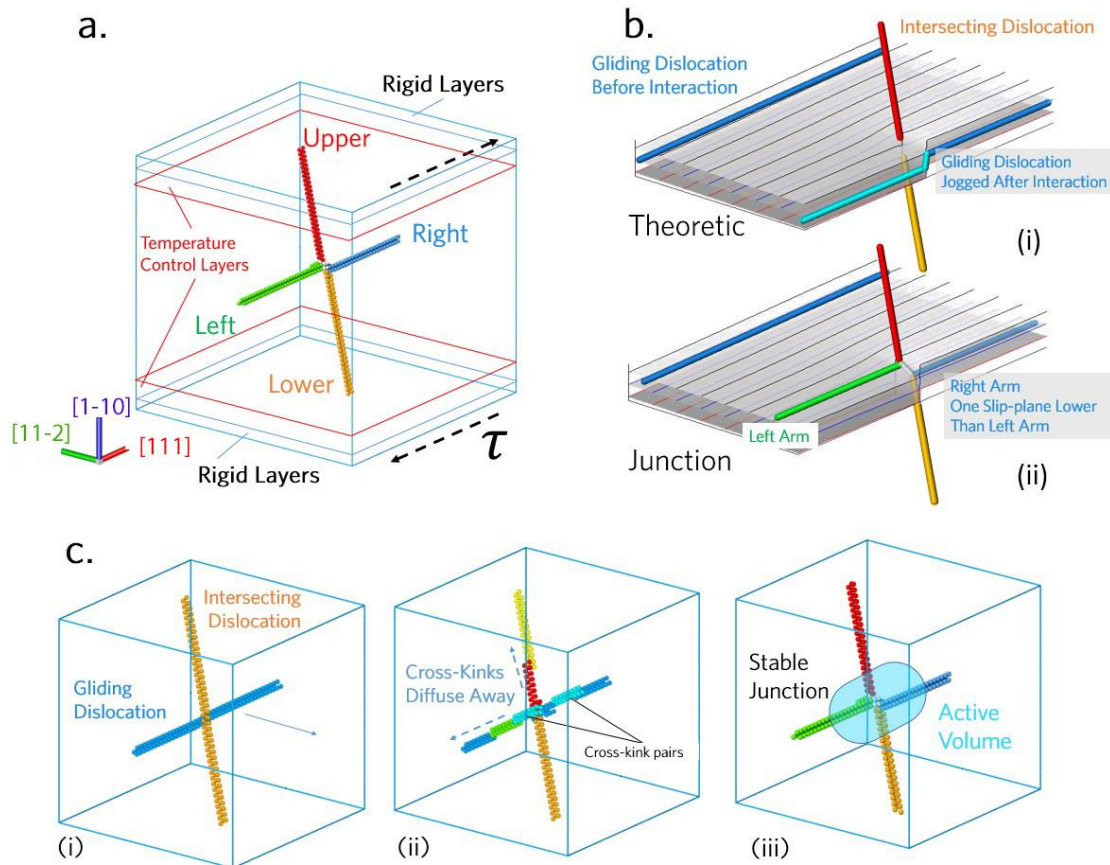
Theoretically, in an infinitely large grain, screw dislocations are unbreakable obstacles to each other. As shown in Fig. 1(b)(i), screw dislocations leave jogs on each other after the interaction, and further dislocation motion requires the jogs to be swept away. However, in the finite-sized grain, kinks or cross-slip kinks can be swept away into grain boundaries or free surfaces with a very small energy barrier, as a screw dislocation tends to keep straight to maintain a low energy state. Thus, in binary junction cases, we use free-boundary conditions in the simulations that contain the junction, which can be an efficient way to represent a finite-size system.

Fig. 1(c) shows the detailed process of stable screw dislocation junction formation in the finite-sized grain. From the beginning, as shown in Fig. 1(c)(i), two separated dislocations are located at far-away distances, with one dislocation (B) intersecting the slip-plane of the gliding dislocation (A). External strain is applied to drive the gliding dislocation on the  $[111]/(1\bar{1}0)$  slip system toward the intersecting dislocation. Note that since in bcc metals the  $\langle 111 \rangle$  screw dislocations with different Burgers vectors are not perfectly vertical, as they approach each other, the gliding dislocation not only migrates via kink-pairs formation but may also cross-slip

as a result of attraction force between the dislocations. Cross-slip kink pairs form in both the intersecting and the gliding dislocation twice (Fig.1(c)(ii)). On the gliding dislocation, the fate of the two cross-slip kinks in the cross-slip kink pair are different: one diffuses towards the intersecting point, combines with another cross-slip kink pair on the intersecting dislocation, and forms the junction. Meanwhile, the other cross-slip kink is swept away along the gliding dislocation into the free surface and disappears. This leads to the stable junction (with the minimum formation energy among all binary junction configurations) in Fig.1(c)(iii). Also, in Fig.1(a), we show the more detailed structure of the obtained junction. The two straight dislocations transform into a junction structure, which consists of four arms. The left arm is located above the right arm by one  $(1\bar{1}0)$  plane.

### **2.3 Molecular Dynamics & Molecular Statics Simulations of Binary Junctions**

In the Molecular Dynamics simulation of the binary junction, we establish a box with  $150 \text{ \AA} \times 150 \text{ \AA} \times 225 \text{ \AA}$ , along  $[112]$ ,  $[11\bar{1}]$ , and  $[1\bar{1}0]$  directions, respectively. The simulation box contains nearly 3 million atoms. Stress is applied to the simulation system by setting several of the top and bottom atomic layers rigid and adding a constant force on the upper rigid layers. The stress is applied to the simulation system before any time-integration algorithm is performed. The constant temperatures are kept by applying the canonical (NVT) ensemble on the temperature control layers next to the rigid layers (the locations of these layers are shown in Fig.1(a)). We applied different temperatures ranging from 50 K to 300 K and a constant 400 MPa shear stress to validate the two of our proposed mechanisms (namely ‘co-planar cross slip’ and ‘unzipping’). Between the upper and lower layers is the dislocation interaction region, in which we applied the NVE ensemble. A third mechanism, (namely ‘jog-pinning’ in later paragraphs) is validated via the athermal molecular statics (MS) simulation. In the MS simulation, a strain is applied by displacing the upper rigid layer along the  $[111]$  direction by small steps of  $0.002 \text{ \AA}$ , followed by the structural minimization using the conjugated gradient (CG) method in the dislocation interaction region. The applied shear strain in the MS simulation is up to 1%, which corresponds to a stress level of nearly 1087 MPa. The MD/MS simulation was carried out with the LAMMPS code [30], and visualization and post-processing were performed using the OVITO [31] software.



**Figure 1:** Schematics of the SPS/MD setup on the screw dislocation junction. **a.** Simulation setup of SPS and MD. **b.** Theoretic behaviors of screw dislocation interaction in infinite-size grain and finite-size grain. (i) For a pure screw dislocation gliding through another screw dislocation with a different Burgers vector, both dislocations leave a jog parallel to their own Burgers vector. Unless the jog slides away or is annihilated at sinks, further gliding of the dislocation will be pinned by the jog, which could substantially increase the stress. (ii) Screw dislocation junction at finite-size grain, with the left arm located one atomic plane higher than the right arm. This is made possible by the annihilation of cross-slip kinks at free surfaces. **c.** (i) Spontaneous formation of the screw dislocation junction. (ii) Extra cross-slip kinks formed as a result of the dislocation interaction and annihilated at free surfaces, which induces (iii) the formation of a stable junction. The blue shades indicate the position and size of the Active Volume used in SPS.

### 3. Results

#### 3.1 Benchmarking Saddle Points of Single Dislocation Motion

To examine the fidelity of SPS results on dislocations by SEAKMC, we conduct SPS of single dislocation motion under stress for two well-established mechanisms: 1) Peierls mechanism, in which a short dislocation overcomes the intrinsic lattice resistance while remaining straight, and 2) kink-pair formation on a long dislocation.

### 3.1.1 Peierls Mechanism

The saddle points identified for a short (with a length of  $5b$ , where  $b$  is the Burgers vector) periodic dislocation are shown in Fig.2. Particularly, six saddle points (marked SP1-6 in Fig.2 (a)) are identified near the non-degenerate compact dislocation core. Fig.2 (a) shows the dislocation movement via SP6. The differential displacement (DD) vectors and Nye tensor field of the initial, saddle, and final configurations are illustrated. The changes of the DD vectors predicted by SEAKMC agree well with previous literature on screw dislocation migration in bcc metals [32,33].

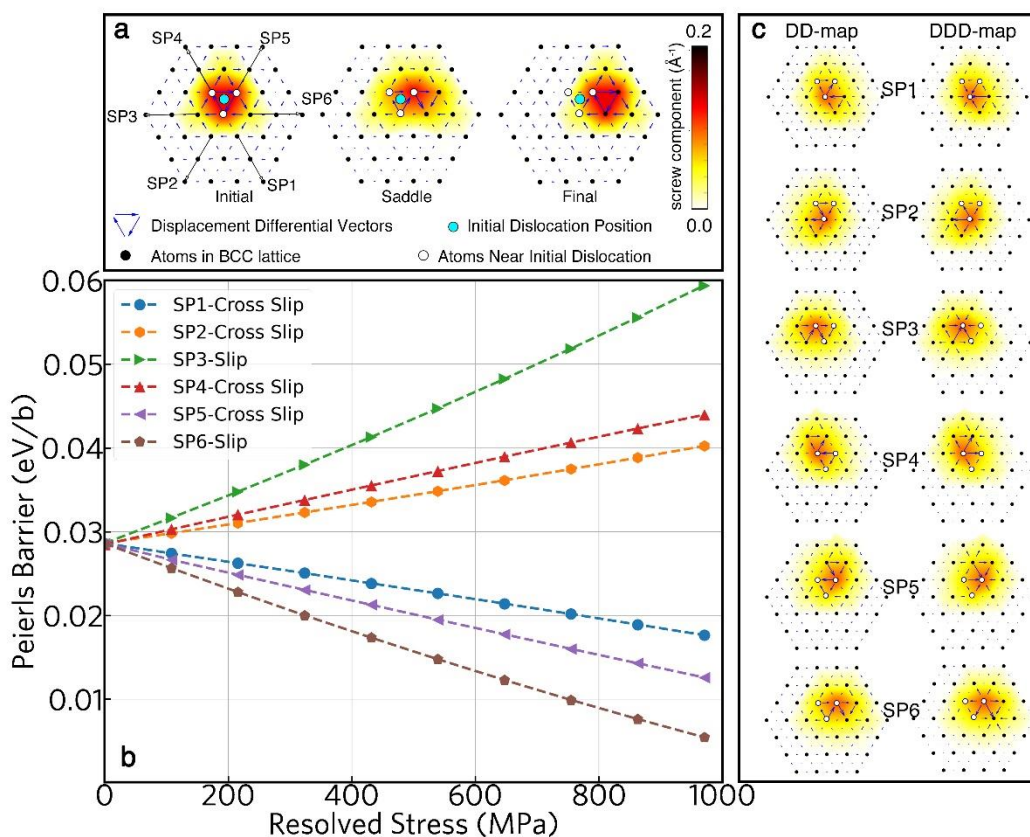


**Figure 2.** Saddle point configurations and their activation energies of a short periodic screw

dislocation. **a.** Initial state, saddle point, and the final state configurations, wherein the dislocation takes SP6 and moves rightward. SP1-6 represents six possible different nearby saddle points, each leading to a different final state. The arrows show the differential displacement fields of the dislocation, and the colored shade indicates the distribution of local screw components of the Nye Tensor [32,34]. **b.** The effects of resolved shear stress on the energy barriers for different saddle points. The external applied resolved stress ranges from 0 to 1000 MPa, which drives the dislocation toward SP6. **c.** Differential displacement map (DD-map) and differences in differential displacement maps (DDD-map) between the six saddle points and the initial configuration.

The effects of the resolved shear stress on the activation energies for the six different saddle points (Peierls Barriers) are shown in Fig. 2(b). The strain is applied by tilting the system, along the  $(1\bar{1}0)$  plane, towards  $\langle 111 \rangle$  (X-direction), resulting in a non-zero  $\sigma_{xz}$  for the system. The  $\langle 111 \rangle / (1\bar{1}0)$  slip system has the maximum resolved shear stress, and the dislocation core is driven towards SP6. Therefore, the reaction paths going through SP6 and SP3 (the direct opposite to SP6) are marked as ‘slip’ events, while the other reaction paths are marked as ‘cross-slip’ events. As expected, the energy of SP6 decreases (and the energy of SP3 increases) with increasing strain. Among the two ‘forward’ cross-slip events (for which the energy barriers decrease with strain), the energy of SP5 decreases faster with strain than SP1. Among the two ‘backward’ cross slip events (for which the energy barriers increase with strain), the energy of SP4 increases more dramatically with strain than SP2. The difference between SP5 and SP1 (as well as between SP2 and SP4) is caused by the twinning/anti-twinning (T/AT) asymmetry [17,33,35-37] of the bcc crystal (which lacks the  $180^\circ$ -rotation symmetry around the  $[111]$  axis). As determined by the potential used in the simulation [13], all saddle points exhibit a core structure between the split-core configurations and the hard-core configurations, and the displacement field of the saddle point with reference to the initial screw dislocation also exhibits 3-fold symmetry, as shown in Fig.2(c).

### 3.1.2 Kink-pair Mechanism

A long screw dislocation tends to glide by a thermally activated, kink-pair nucleation and propagation mechanism ('kink-pair mechanism' in short), as observed previously from atomistic simulations and TEM experiments [10,11,13,17]. Here we conduct SPS for a dislocation with a  $100b$  length to obtain the saddle point of the kink-pair mechanism. SPS is carried out using a predefined capsule-shaped *active volume* (AV, See Methodology section), with its long axis along the dislocation line, i.e.  $[111]$  direction. The *active volume* includes  $\sim 20000$  atoms. The strain condition is the same as that in the Peierls mechanism simulations. Six different saddle points were found and are categorized as 'kink-pairs' (SP3,6) and 'cross-slip kink pairs' (SP1,2,4,5), according to the direction of dislocation migration [17]. The atomistic configurations of the saddle points are shown in Fig. 3 (b).

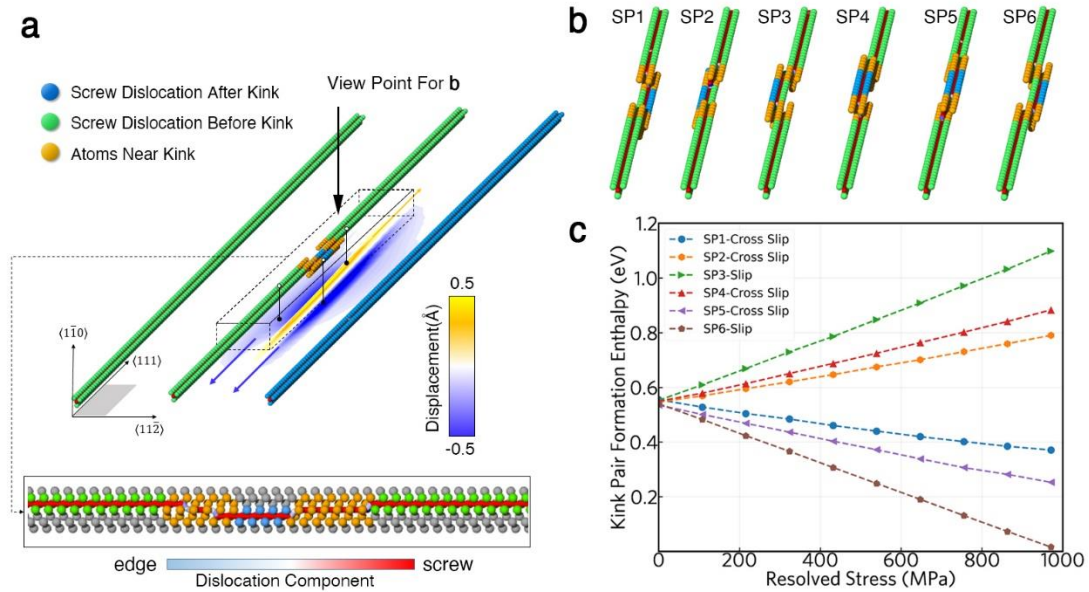


**Figure 3.** **a.** Schematics for the kink-pair mechanism. Only atoms around the dislocation core are shown. Atoms around the dislocation segment that do not move are colored green. Atoms around the dislocation segment that has moved forward by one lattice spacing are colored blue. Atoms connecting these segments (i.e. around the kinks) are colored orange. The shades beneath the saddle point configuration show the atomistic displacements relative to the initial configuration. The dislocation configuration at the saddle point is shown in the expanded figure below. **b.** Atomistic configurations of six saddle points, corresponding to the kink-pair

formation from the initial configuration toward six different  $[112]$  directions. **c.** The energies of the six-saddle points as a function of applied strain.

To our knowledge, this is the first open-ended search of saddle points for a long screw dislocation that successfully identifies the kink-pair and cross-slip kink-pair mechanism without prior knowledge (e.g., the construction of an initial path in the NEB method). The yellow-blue shade in Fig. 3(a) shows the atomistic displacement along the Burgers vector direction at the saddle point with respect to the initial dislocation. The maximum atomistic displacement at the saddle point is around  $0.68 \text{ \AA}$ , which is nearly one-fourth of the Burgers vector. A very low energy barrier for kink migration ( $< \sim 0.01 \text{ eV}$ ) is also found by SPS. Therefore, once the kink-pair forms by thermal fluctuation, the kinks are expected to rapidly glide away from each other, moving the entire dislocation to the next lattice position. The effects of applied shear stress on the six saddle points are shown in Fig. 3(c). The SPS result under zero-stress conditions gives kink-pair formation energy of  $0.58 \text{ eV}$ , which agrees well with the NEB calculated result [13]. Furthermore, the formation enthalpy of kink-pairs along SP6 decreases the fastest with the applied shear stress. It results in a Peierls stress of nearly  $1.0 \text{ GPa}$ , which is consistent with the prediction by the line-tension (LT) model [38].

### **3.2 Multi-mechanisms of screw dislocation binary junction under stress**

Fig. 4(a) shows a schematic of the binary junction, formed by two screw dislocations with  $\mathbf{b}_1 = \frac{1}{2}[111]$  and  $\mathbf{b}_2 = \frac{1}{2}[\bar{1}\bar{1}\bar{1}]$ . The junction structure is created by applying a shear stress  $\sigma_{xz}$  to drive the gliding dislocation (with the Burgers vector  $\mathbf{b}_1$ ) toward the  $[\bar{1}\bar{1}2]$  direction to the intersecting dislocation (with the Burgers vector  $\mathbf{b}_2$ ). After the two dislocations meet, a short junction segment with a Burgers vector  $[010]$  is formed. Due to the interaction geometry of the two dislocations in the binary junction, the left arm of the dislocation is one atom-plane above the right arm (as discussed in the methodology section).

Based on SPS results, we find the saddle points on the left and right arms determine the possible evolution of the junction. According to obtained saddle points, we propose three possible

scenarios: *coplanar cross-slip* (CPCS), *jog-pinning*, and an *unzipping* mechanism, as shown in Fig.4(b)-(d), respectively. CPCS occurs when both arms choose to cross-slip downwards by one atomic plane, maintaining an equivalent geometry with the initial configuration. Comparatively, *jog-pinning* occurs when both arms continue to move forward, and neither arm changes its slip-plane. Since they are not located on the same slip-plane, a jog, which is geometrically necessary, will be left at its original position and pins the gliding dislocation. In later paragraphs of this section, we introduce in detail the discovered saddle points of binary junctions and their relationship with the above scenarios.

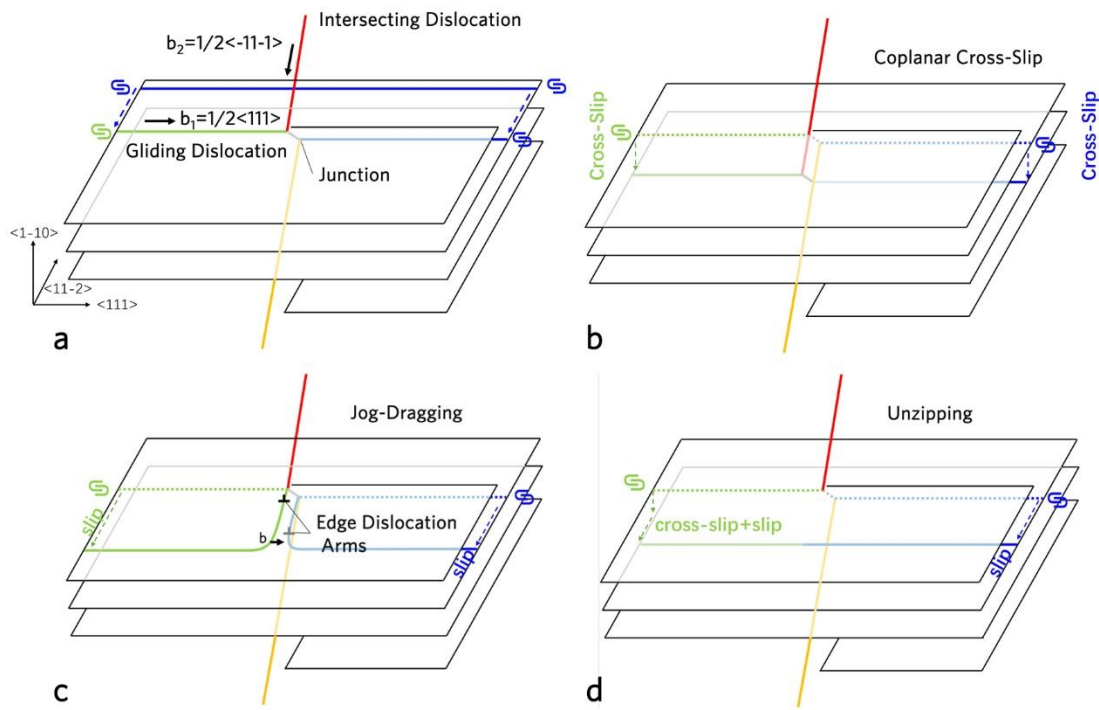


**Figure.4** Schematics on the formation of screw dislocation binary junction and possible scenarios of evolution under stress. **a.** Dislocation configurations of binary junctions and those before the formation of the junction. **b.** CPCS when both arms cross-slip downwards. **c.** Jog pinning occurs when neither of the left nor right arms cross-slip. **d.** The unzipping scenario occurs when only the left arm cross-slips downwards by one plane. Then, after the gliding dislocation unzips the junction, a jog is left on the intersecting dislocation that connects the yellow and red segments.

Particularly, based on the junction structure shown in Fig.5(a), our SPS finds three saddle points on the left arm and two on the right arm. The atomic structures of these saddle points and their corresponding final states are shown in Fig. 5(b). The events leading to dislocation motion in the  $[1\bar{1}2]$  direction is considered to be a ‘*kink-pair*’ formation and labeled as  $K^{left}$  and  $K^{right}$  depending on whether it occurs on the left or right arm, respectively. Otherwise, events that lead to dislocation motion in other directions are considered ‘*cross-slip kinks*’ and are labeled as  $C_{low}^{left}$ ,  $C_{low}^{right}$ ,  $C_{up}^{left}$ , according to the dislocation moving direction and their positions, as shown in Fig. 5(b). The event that corresponds to  $C_{up}^{right}$  has not been found on the right arm, indicating it is probably energetically unfavorable or it is unlikely to occur near binary junctions.

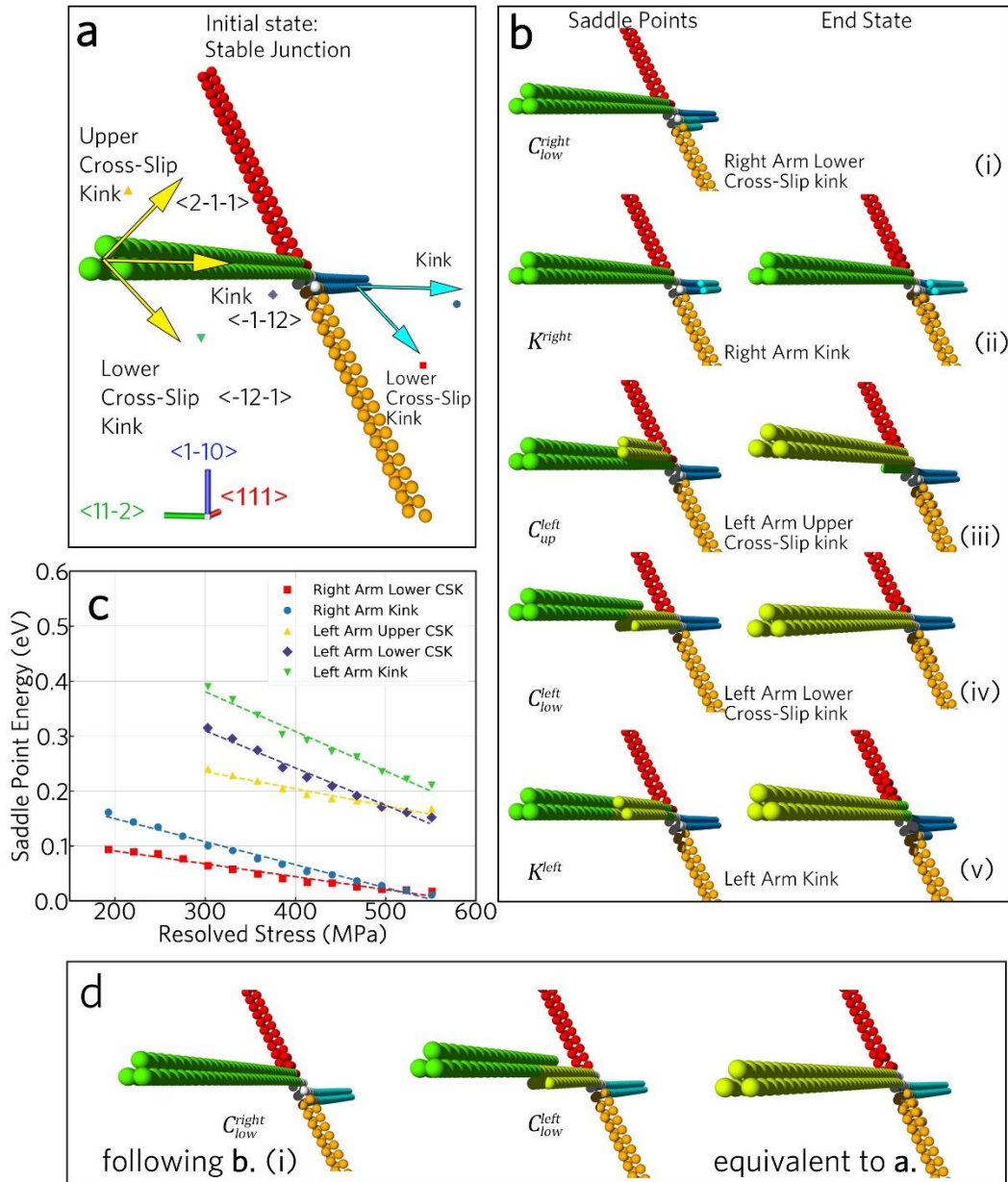


**Figure 5. a.** The structure of a dislocation junction, which is also the initial configuration for SPSs. The gliding dislocation ( $\mathbf{b} = \frac{1}{2}\langle 111 \rangle$ , slip plane  $(1\bar{1}0)$ ), zipped with an intersecting dislocation ( $\mathbf{b} = \frac{1}{2}\langle 1\bar{1}\bar{1} \rangle$ ). A junction consists of four arms (left and right arms for the moving dislocation and upper and lower arms for the intersecting dislocation). The yellow/cyan arrows indicate the direction of kinks and cross-slip kinks formed at the left (green) and right (blue) arms. **b.** Structures of saddle points correspond to kink or cross-slip kink formation at both left and right arms; **c.** Stress effect on the activation energies of the kinks or cross-slip kinks on the left- and right- arms. **d.** The initial configuration, saddle point, and final configuration of the

*co-planar cross slip* mechanism following the structure shown in **b**.

The stress dependencies of the formation energies of the above five saddle points are shown in Fig. 5(c). Due to the formation of the binary junction, the activation energies of the right-arm events are significantly lower than those on the left arm. Thus, the right-arm events are supposed to occur earlier at the same stress/temperature condition than those on the left arm. The kink-pairs, or the cross-slip kink pairs on the right-arm also have lower activation energies than those on a single dislocation. Thus, the formation of binary junctions promotes the formation of kink-pairs and cross-slip kink pairs on the right arm. The  $K^{right}$  event has higher energy than the  $C_{low}^{right}$  event at lower stresses, but decreases faster with stress, leading to a crossover of the two events at a stress level of around 525 MPa. Thus, at low temperatures, the  $C_{low}^{right}$  event plays a predominant role at low stresses. Nonetheless, the activation energies for  $K^{right}$  and  $C_{low}^{right}$  events are relatively close, which indicates that rate of occurrence of  $K^{right}$  and  $C_{low}^{right}$  can be close at high temperatures.

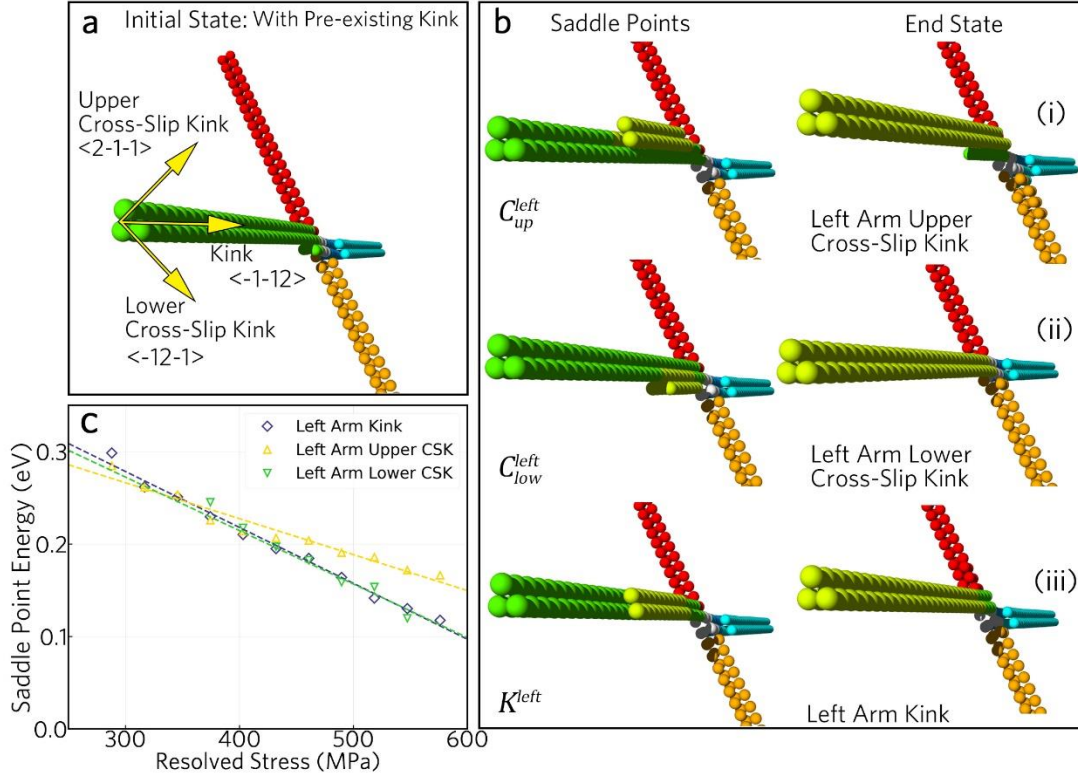


**Figure 6.** SPS search performed on a screw dislocation junction with a pre-existing kink on the right-arm. The initial configuration is obtained following a right-arm kink event ( $K^{right}$ ) in Fig. 5 (b,ii). **a.** Directions of kinks or cross-slip kinks formed on the left arm. Due to the existing kink, other kinks or cross-slip kinks become harder to nucleate on the right arm. **b.** Structures of saddle points correspond to kink or cross-slip kink formation on the left arm. **c.** Influence of stress on the formation energy of the kinks or cross-slip kinks on the left arm.

We choose two end configurations from the right-arm events (Fig.5(b)(i) and (ii)) to find their subsequent saddle point after the first event has taken place. Since the left-arm events in Fig.5 have significantly higher barriers than that of the right arms, we assume the right-arm events occur ahead of the left-arm events. Therefore, we do not use the final states of the left-arm event in Fig.5 as initial configurations of the following SPS.

First, starting from the resultant configuration of  $C_{low}^{right}$  as shown in Fig.5(b)(i), SPSs only find one event:  $C_{low}^{left}$  shown in Fig.5(d) with a negligible energy barrier, leading to a structure

that maintains the same symmetry as the initial configuration shown in Fig.5(a). This is how the CPCS mechanism takes place [7].

Second, the SPS results starting from the resultant configuration of  $K^{right}$  as shown in Fig.5(b)(ii) are presented in Fig.6. Following the  $K^{right}$  event in Fig.6(a), SPSs on the right arm find no relevant saddle points, but SPSs on the left arm identified three different saddle point configurations, labeled as  $K^{left}$ ,  $C_{low}^{left}$ , and  $C_{up}^{left}$ , leading to three separate end states.

As shown in Fig.6(b), with  $C_{up}^{left}$ , the left arm is two atomistic planes above the right arm, with  $C_{low}^{left}$ , the left arm moves down to the same atomic plane as the right arm. By  $K^{left}$  the left arm moves forward, remaining above the right arm by one slip plane.

The barriers of all these events decrease as external stress increases. According to Fig.6(c),  $C_{up}^{left}$  has a higher activation energy and decreases much slower with stress than  $K^{left}$  and  $C_{low}^{left}$ . Activation energies of  $K^{left}$  and  $C_{low}^{left}$  are similar, and so are their dependencies on stresses. These events lead to different junction behaviors:  $K^{left}$  marks the beginning of the jog-pinning mechanism, and  $C_{low}^{left}$  aligns both arms on the same slip-plane, thereby enabling the junction to unzip. Thus, different combinations of the left and right arm events, lead to different behaviors of the binary junction under stress.

We again summarize how the critical kink and cross-lip kink events determine which mechanism to take for the junction, in **Table I**: (1)  $(C_{low}^{right}, C_{low}^{left})$ : CPCS mechanism, the sliding dislocation is moving in the cross-slip direction along Burgers vector of the *intersecting dislocation*. (2)  $(K^{right}, K^{left})$ : *Jog-pinning mechanism*, where a jog is created as an unbreakable obstacle; (3)  $(K^{right}, C_{low}^{left})$ , a previously unreported *unzipping* mechanism, where the cross-slip of the left arm enables the gliding dislocation to detach from the intersecting dislocation. The presence of this mechanism indicates the screw dislocation is able to unzip the intersecting dislocation without leaving behind debris composed of point defects.

**Table I:** Combination of events on the right and left arms, which determines the behavior of

the binary junction.

Right Arm Event	Left Arm Event	Resultant Mechanism
$C_{low}^{right}$	$C_{low}^{left}$	Coplanar Cross Slip
	$K^{left}, C_{up}^{left}$	Jog-pinning
$K^{right}$		
	$C_{low}^{left}$	Unzipping

### **3.3 Validation of These Mechanisms using Molecular Dynamics**

To validate the mechanisms proposed based on the SPS, we conduct classical MD and MS on the junction structure. For the validation of the jog-pinning mechanism, the molecular statics (MS) simulation with increasing shear stress is conducted. Details of computational settings are presented in the Methodology section. The results are shown in Fig.7. In the MS simulations, the junction structure may only evolve athermally into a new state when the barrier becomes close to zero due to the increasing stress. Thus, when the stress reaches around 600 MPa, a kink-pair spontaneously forms on the right arm near the junction. As shown in the snapshots in Fig.7(a), no thermal-activated events occur as the stress increases. The left and right arms are kept at their original slip-plane. As they move forward, a jog is dragged behind them, then forming a dipole loop[39] as the dislocation gets far from the junction.

Equilibrium MD simulations are performed with the temperature and stress kept constant. The shear stress is kept 400MPa. In the MD simulation at 200 K as shown in Fig.7(b), the gliding dislocation cross-slips along the mutual slip-plane of the intersecting dislocation. It only takes the CPCS mechanism and does not leave the intersecting dislocation. At 300 K, however, the gliding dislocation first takes the CPCS mechanism; after cross-slipping for a few steps, it

leaves the intersecting dislocation via the thermal-activated unzipping mechanism. In the MD/MS simulation, all three proposed mechanisms are validated.

## 4. Discussion

The above SPS and MD results reveal a remarkable feature of the junction: the junction significantly reduces the formation energies of kink-pairs and cross slip kink-pairs, especially at the right arms. Furthermore, competitions among several events near junctions and events far away from junctions (mostly kink-pair formation) significantly influence the evolution mechanisms. These competitions have profound implications on the temperature dependence of junction behaviors.

### 4.1 Competitions among events near binary junctions.

At zero temperature, the MS simulation reveals that the Peierls stress of the right arm of the junction is reduced in comparison with the Peierls stress of a single straight screw dislocation. It thus implies that, at very low temperatures, the evolution of the binary junction starts with the kink-pair formation near the junction, instead of kink-pair formation on the straight screw dislocation segments far away from the junction.

At a finite temperature, close to the binary junction, the energy barriers of both the  $C_{low}^{right}$  and  $K^{right}$  are rather low, though the energy barrier of  $C_{low}^{right}$  is lower. This indicates that at low temperatures when the  $\sim 0.2$  eV energy cannot be not easily overcome, the  $C_{low}^{right}$  event dominates, and the junction mostly takes the CPCS mechanism. In comparison, when the temperature rises to room temperature, both  $C_{low}^{right}$  and  $K^{right}$  events occur, leading to the unzipping mechanism. Thus, the overall effect of the competition between the CPCS and the unzipping mechanism leads to the suppression of CPCS at high temperatures, which is in agreement with our MD simulation.

### 4.2 Competitions between near-junction events and far away events

Furthermore, the competition between the near-junction events and events far away from the junction may also lead to different behavior at finite temperatures. Although the kink-pair formation energy at faraway segments is higher than those near the junctions, there are more locations of the kink-pair nucleation at dislocation segments far away from the junction. Thus, the overall occurrence of the kink-pair formation may linearly increase with the length of the straight segments. This indicates that at low temperatures when near-junction events are dominating, the junction mostly takes the near-junction events (which is mostly CPCS). At high temperatures, the overall occurrence of kink-pair formation far away from the junctions may be higher than the CPCS mechanism, and kink-pairs may form far away from the junction before the formation of cross slip kinks near the junction. Once the kink-pairs form at far-away distances from the junction, one of the kinks in the pair may quickly diffuse towards the junction and form a structure like those shown in Fig.5(b) (ii or v). According to our results, a kink near the junction on one arm tends to suppress the formation of cross-slip kinks on that arm. Thus, the kink-pairs forming at far away distances from the junctions eventually suppress other near-junction events. Thus, competition between near-junction events and far-away events leads to reduced activity of CPCS at high temperatures.

### **4.3 Implications to the anomalous slip phenomenon**

According to the above discussion and our SPS/MD results, the atomistic behavior described in this paper can be directly linked to the anomalous slip phenomenon in BCC metals. In our simulations, the primary slip system is  $[111]/(1\bar{1}0)$  and the CPCS system is  $[111]/(\bar{1}01)$ . CPCS is the most probable mechanism taken by the junction at below 200 K. It is thus a significant violation of the Schmidt law. At higher temperatures however, the primary slip system is activated by either the unzipping mechanisms near the junction or the kink-pair formation mechanisms at straight segments far away from the junctions, the CPCS is then suppressed. Such behavior agrees with the low-temperature anomalous slip phenomenon in bcc metals and its suppression at high temperatures. There is currently no report on the anomalous slip phenomenon in bcc Fe [40]. However, this manuscript reports a model study based on interatomic potential. And due to the transferability of the simple analytical form of EAM potential, we believe the saddle points and mechanisms can also be generalized to other bcc

metals, to explain the atomistic mechanism and temperature dependency of the anomalous slip phenomenon.

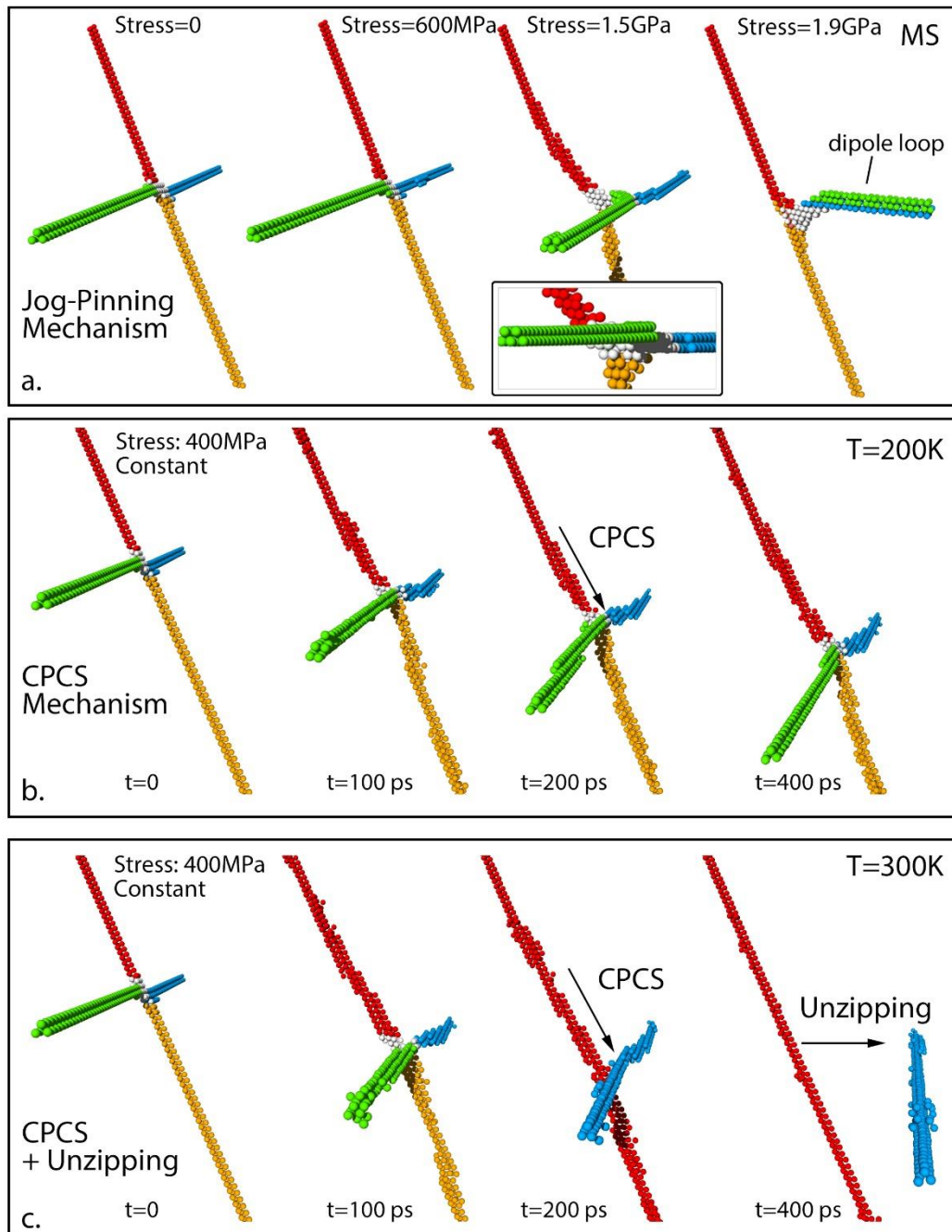


Fig. 7 MD (MS) simulation revealing the jog-pinning, CPCS, and unzipping mechanisms. (a) In the MS simulation, the junction takes the stress-driven jog-pinning mechanism. (b) In MD simulation at 200 K, the gliding dislocation only takes the CPCS mechanism. At 300 K, the gliding dislocation first takes CPCS and cross-slips for a short distance, then the unzipping

mechanism occurs (the gliding dislocation passes the intersecting dislocation).

## **Summary**

It is well known that the interaction between dislocations contributes substantially to the overall plastic deformation in metallic materials. Resolving the atomistic mechanisms in dislocation interactions is critical to the further evaluation of strain hardening. Here we develop and demonstrate a computational capability with atomistic resolution and meso- (experimental) timescales. Using this method, we find three competing mechanisms of a binary junction that drive the gliding dislocations on the  $\langle 111 \rangle / (1\bar{1}0)$  slip system under stress, namely: the coplanar cross-slip mechanism, the jog-pinning mechanism, and the unzipping mechanism. The unzipping mechanism has not been found in the past and identifying it together with other mechanisms demonstrates the complexity of the potential landscape associated with a binary junction. We further reveal that the choice of thermally activated events occurring on the sliding dislocation near the junction play a critical role in dictating which mechanism occurs under different conditions, leading to different stress-strain responses to external stimuli. All these mechanisms are then confirmed using MD at different temperatures. The activation energies of various events, and the influence of stresses on the activation energies, are established. These results can be extended to other BCC metals to explain the anomalous slip phenomenon and can also provide essential input mechanisms to large-scale modeling simulation techniques.

## **Acknowledgement**

Work at UTK was supported by the U.S. Department of Energy (DOE), Office of Science, Basic Energy Sciences (BES), under Award No. DE-SC0019151. Work at Stanford was supported by DOE, Office of Science, BES, Division of Materials Sciences and Engineering under Award No. DE-SC0010412. This research used resources of the National Energy Research Scientific Computing Center, a DOE Office of Science User Facility supported by the Office of Science of the DOE under Contract No. DE-AC02-05CH11231.

**No Competing Interests Statement**

The authors declare that there are no competing interests.

**Data Availability Statement**

The data generated during and/or analyzed during the current study are available from the corresponding author upon reasonable request.

**Author Contribution**

H.X. conceived and led the work. X.W. performed the simulations, collect the data, and wrote the initial manuscript. X.W., Y.W, W.C., and H.X. analyzed the results and revised the manuscript.

## REFERENCES

- [1] S. M. Hafez Haghghat, R. Schäublin, and D. Raabe, Atomistic simulation of the  $a_0$   $\langle 100 \rangle$  binary junction formation and its unzipping in body-centered cubic iron, *Acta. Mater.* **64**, 24 (2014).
- [2] S. Queyreau, G. Monnet, and B. Devincre, Slip systems interactions in  $\alpha$ -iron determined by dislocation dynamics simulations, *Int. J. Plast.* **25**, 361 (2009).
- [3] V. V. Bulatov *et al.*, Dislocation multi-junctions and strain hardening, *Nature* **440**, 1174 (2006).
- [4] A. Arsenlis, W. Cai, M. Tang, M. Rhee, T. Ooppelstrup, G. Hommes, T. G. Pierce, and V. V. Bulatov, Enabling strain hardening simulations with dislocation dynamics, *Model. Simul. Mat. Sci. Eng.* **15**, 553 (2007).
- [5] T. Jogi and S. Bhattacharya, Interfacial dislocation network in precipitation strengthened alloys during creep: a discrete dislocation dynamics (DDD) study in three dimensions, *Model. Simul. Mat. Sci. Eng.* **29**, 035010 (2021).
- [6] R. Kapoor and N. Verdhan, Interaction of dislocation pile-up with a low-angle tilt boundary: a discrete dislocation dynamics study, *Philos. Mag.* **97**, 465 (2017).
- [7] V. V. Bulatov and W. Cai, Nodal Effects in Dislocation Mobility, *Phy. Rev. Lett.* **89**, 115501 (2002).
- [8] Z. Y. Xia, Z. J. Zhang, J. X. Yan, J. B. Yang, and Z. F. Zhang, Simulation of the interaction between two different  $1/2\langle 111 \rangle$  screw dislocations in body-centered-cubic metal niobium, *Comput. Mater. Sci.* **174**, 109503 (2020).
- [9] M. Trochet, N. Mousseau, L. K. Béland, and G. Henkelman, Off-lattice kinetic Monte Carlo methods, *Handbook of Materials Modeling: Methods: Theory and Modeling*, 715 (2020).
- [10] C. Domain and G. Monnet, Simulation of Screw Dislocation Motion in Iron by Molecular Dynamics Simulations, *Phy. Rev. Lett.* **95**, 215506 (2005).
- [11] D. Caillard, Kinetics of dislocations in pure Fe. Part I. In situ straining experiments at room temperature, *Acta. Mater.* **58**, 3493 (2010).
- [12] Y. Fan, A. Kushima, S. Yip, and B. Yildiz, Mechanism of Void Nucleation and Growth in bcc Fe: Atomistic Simulations at Experimental Time Scales, *Phy. Rev. Lett.* **106**, 125501 (2011).
- [13] L. Proville, D. Rodney, and M.-C. Marinica, Quantum effect on thermally activated glide of dislocations, *Nat. Mater.* **11**, 845 (2012).
- [14] A. Seeger and U. Holzwarth, Slip planes and kink properties of screw dislocations in high-purity niobium, *Philos. Mag.* **86**, 3861 (2006).
- [15] D. Brunner, Comparison of flow-stress measurements on high-purity tungsten single crystals with the kink-pair theory, *Mater. Trans.* **41**, 152 (2000).
- [16] A. F. Voter, F. Montalenti, and T. C. Germann, Extending the time scale in atomistic simulation of materials, *Ann. Rev. Mater. Res.* **32**, 321 (2002).
- [17] A. Stukowski, D. Cereceda, T. D. Swinburne, and J. J. I. J. o. P. Marian, Thermally-activated non-Schmid glide of screw dislocations in W using atomistically-informed kinetic Monte Carlo simulations, *Int. J. Plast.* **65**, 108 (2015).
- [18] H. Xu, Y. N. Osetsky, and R. E. Stoller, Self-evolving atomistic kinetic Monte

- Carlo: fundamentals and applications, *J. Phys. Condens. Matter* **24**, 375402 (2012).
- [19] H. Xu, Y. N. Osetsky, and R. E. Stoller, Simulating complex atomistic processes: On-the-fly kinetic Monte Carlo scheme with selective active volumes, *Phy. Rev. B* **84**, 132103 (2011).
- [20] X. Yan and P. Sharma, Time-Scaling in Atomistics and the Rate-Dependent Mechanical Behavior of Nanostructures, *Nano Letters* **16**, 3487 (2016).
- [21] Y. Fan, Y. N. Osetskiy, S. Yip, and B. Yildiz, Mapping strain rate dependence of dislocation-defect interactions by atomistic simulations, *PNAS*, **110**, 17756 (2013).
- [22] G. Henkelman and H. Jónsson, Improved tangent estimate in the nudged elastic band method for finding minimum energy paths and saddle points, *J. Chem. Phys.* **113**, 9978 (2000).
- [23] G. Henkelman, B. P. Uberuaga, and H. Jónsson, A climbing image nudged elastic band method for finding saddle points and minimum energy paths, *J. Chem. Phys.* **113**, 9901 (2000).
- [24] Z. Bai and Y. Fan, Abnormal strain rate sensitivity driven by a unit dislocation-obstacle interaction in BCC Fe, *Phy. Rev. Lett.* **120**, 125504 (2018).
- [25] Y. Fan, Y. N. Osetsky, S. Yip, and B. Yildiz, Onset Mechanism of Strain-Rate-Induced Flow Stress Upturn, *Phy. Rev. Lett.* **109**, 135503 (2012).
- [26] A. Ervin and H. Xu, Mesoscale simulations of radiation damage effects in Materials: A SEAKMC perspective, *Comput. Mater. Sci.* **150**, 180 (2018).
- [27] H. Xu, R. E. Stoller, Y. N. Osetsky, and D. Terentyev, Solving the puzzle of  $\langle 100 \rangle$  interstitial loop formation in bcc Iron, *Phys. Rev. Lett.* **110**, 265503 (2013).
- [28] S. Hayakawa, J. Isaacs, H. R. Medal, and H. Xu, Atomistic modeling of meso-timescale processes with SEAKMC: A perspective and recent developments, *Comput. Mater. Sci.* **194**, 110390 (2021).
- [29] G. Henkelman and H. Jónsson, A dimer method for finding saddle points on high dimensional potential surfaces using only first derivatives, *J. Chem. Phys.* **111**, 7010 (1999).
- [30] S. Plimpton, Fast Parallel Algorithms for Short-Range Molecular Dynamics, *J. Comput. Phys.* **117**, 1 (1995).
- [31] A. Stukowski, Visualization and analysis of atomistic simulation data with OVITO – the Open Visualization Tool, *Model. Simul. Mat. Sci. Eng.* **18**, 015012 (2009).
- [32] B. G. Mendis, Y. Mishin, C. S. Hartley, and K. J. Hemker, Use of the Nye tensor in analyzing HREM images of bcc screw dislocations, *Philos. Mag.* **86**, 4607 (2006).
- [33] L. Ventelon, F. Willaime, E. Clouet, and D. Rodney, Ab initio investigation of the Peierls potential of screw dislocations in bcc Fe and W, *Acta Mater.* **61**, 3973 (2013).
- [34] F. Dai and W. J. A. M. S. Zhang, Identification of secondary dislocations by singular value decomposition of the Nye tensor, *Acta Metall. Sin-Engl.* **27**, 1078 (2014).
- [35] L. Dezerald, D. Rodney, E. Clouet, L. Ventelon, and F. J. N. c. Willaime, Plastic anisotropy and dislocation trajectory in BCC metals, *Nat. Commun.* **7**, 1 (2016).
- [36] G. Po, Y. Cui, D. Rivera, D. Cereceda, T. D. Swinburne, J. Marian, and N. Ghoniem, A phenomenological dislocation mobility law for bcc metals, *Acta Mater.* **119**, 123

(2016).

[37]A. Kraych, E. Clouet, L. Dezerald, L. Ventelon, F. Willaime, and D. Rodney, Non-glide effects and dislocation core fields in BCC metals, *npj Comput. Mater.* **5**, 109 (2019).

[38]L. Proville, L. Ventelon, and D. Rodney, Prediction of the kink-pair formation enthalpy on screw dislocations in  $\alpha$ -iron by a line tension model parametrized on empirical potentials and first-principles calculations, *Phys. Rev. B* **87**, 144106 (2013).

[39]H. Matsui and H. Kimura, Anomalous  $\{110\}$  slip in high-purity molybdenum single crystals and its comparison with that in V (a) metals, *Mater. Sci. Eng.* **24**, 247 (1976).

[40]Z. Chen, M. Mrovec, and P. Gumbsch, Atomistic aspects of screw dislocation behavior in  $\alpha$ -iron and the derivation of microscopic yield criterion, *Model. Simul. Mat. Sci. Eng.* **21**, 055023 (2013).